

# Study of influence of additive wire-arc manufacturing modes on microstructure of AA7075 alloy

**I. A. Panchenko**, Candidate of Technical Sciences, Head of the Laboratory of Electron Microscopy and Image Processing<sup>1</sup>, e-mail: i.r.i.ss@yandex.ru

**D. A. Bessonov**, Candidate of Technical Sciences, Senior Researcher<sup>1</sup>, e-mail: dabess@yandex.ru

**S. V. Konovalov**, Professor<sup>1</sup>, Doctor of Technical Sciences, Vice-Rector for Research and Innovation, e-mail: konovalov@sibsiu.ru

**D. N. Labunsky**, Post-Graduate Student<sup>1</sup>, e-mail: info@kana-t.ru

<sup>1</sup> Siberian State Industrial University, Novokuznetsk, Russia.

The article discusses the wide application of aluminum alloys in various industries, as well as the necessity to increase their strength to meet the requirements of modern technologies. An important point is to investigate the evolution of nanoscale precipitates in AA7075 alloy, in order to improve the mechanical properties of the material. Manufacturing of aluminum alloy parts by additive method allows you to achieve a high level of productivity and, if necessary, to exceed mechanical standards for these materials. Particular attention is paid to structural phase state studies, which are necessary for the development of new technologies based on additive manufacturing, such as surface cladding of aluminum alloys. The study showed that the surface cladding mode (Ar flow rate  $\approx 10$  l/min, surface cladding speed 100 mm/min, current — 70–80 A, voltage — 15.8 V, wire feed speed — 4 m/min) provides the best results in terms of quality and stability of the cladding process. The manufactured blanks had a dense structure with no visible cracks and the porosity percentage was low. This indicates to the possibility of using this mode for the production of high-quality cladding materials. The MIG welding process using constant optimal technological parameters allows to obtain aluminum alloy AA7075 with desired microstructural properties by additive manufacturing method. Strengthening phases in the alloy help prevent crack growth during mechanical testing, and the morphology of equiaxed grains may contribute to uniform stress distribution and increase the strength of the material. It is important to note that large columnar grains in the fusion zones can affect the mechanical properties of the material and additional studies may be required to determine their effect on the overall strength of the alloy.

**Key words:** aluminum alloys, properties, additive technologies, materials, surface cladding, structure, mechanical tests, strengthening phases.

**DOI:** 10.17580/nfm.2024.02.13

## Introduction

Aluminum alloys are widely used in automotive, electronics, marine and defense industries due to their high mechanical properties and high machinability, as well as high electrical conductivity, high corrosion resistance and weldability, low density and fatigue resistance. AA7075 alloy is an important and indispensable material in the aviation industry which has reliable properties, especially for airplane wing pylons, airframes and rocket construction. However, despite the wide range of applications, industrial uses of aluminum alloys require even higher strengths to meet their specific requirements [1, 2].

The transportation industry is under increasing pressure of the necessity to improve the fuel economy and safety of vehicles. Among a large number of research papers on the properties of ferrous and non-ferrous metals, aluminum alloys occupy a significant place due to their high combination of mechanical properties and low structural weight [3, 4].

Nowadays, additive technologies are finding more and more applications. There are a number of reasons for this, the key of which are the possibility of manufacturing

structures that could not be produced by classical methods, also one of the important factors is the reduction of time to bring the product-structure to the market due to the possibility of rapid production, the fact of obtaining unique properties of the structure due to the application of a new principle of production is also important. In most cases, various types of plastics are used in additive manufacturing, but metal printing is also important for the development of additive technologies. Solid-state additive manufacturing is a promising technology for producing alloys with complex geometries for aerospace applications [5]. Among additive metal production technologies, additive friction stir deposition (AFS-D) is an innovative solution for fabricating and repairing high-strength aluminum alloy components [6]. The material is applied layer by layer using a hollow rotating tool to the substrate material [7]. When the hollow rotating tool comes into contact with the substrate, heat and friction pressure are generated which create a metallic bond between the feed material and the substrate. In AA7075 alloy, nanoscale  $\text{MgZn}_2$  ( $\eta'$ ) and  $\text{MgZn}_2(\eta)$  precipitates control the strength of

the material and can be dissolved and reformed using the AFS-D thermomechanical process. The study investigates the evolution of grain size, phase composition and spatial distribution of nanoscale precipitates in deposited and heat-treated AA7075 material.

Additive manufacturing of parts based on aluminum alloys allows growing with very high productivity. At the same time, it is worth noting that the resulting products can have mechanical properties higher than the state standards for the same alloy.

In the last decade, aluminum alloys [8–10] and aluminum-matrix materials reinforced with SiC particles [11–15], Al<sub>2</sub>O<sub>3</sub> [16, 17], B<sub>4</sub>C [18–20], Si<sub>3</sub>N<sub>4</sub> [21, 22] have expanded their applications, and carbon nanotubes [23, 24] have become significantly widespread. Such materials are used as structural materials in aerospace [16, 24], electronics [23], automotive [25, 26], military [27], and others. The share of aluminum-matrix materials in the total volume of structural materials of functional parts is constantly increasing. This trend is explained by the unique mechanical and thermoelectric properties of materials with aluminum matrix in combination with low weight [28]. In addition, the functional properties of materials with aluminum matrix can be adjusted by varying the amount, size, shape and type of reinforcing inclusions [29, 30].

**Purpose of work** — Study of structural-phase state of surface cladding layers of aluminum alloy grade 7075, produced by wire-arc surface cladding using additive manufacturing technologies.

### Materials and methods

AA7075 alloy specimens were produced in the facilities of the “Welding Processes and Technologies” R&D

Table 1  
Chemical composition of aluminum wire, wt. %

Study Material	Al	Si	Fe	Mn	Cu	Mg	Cr	Zn	Ti
AA7075 wire	balance	0.4	0.1	0.3	1.6	2.51	0.18	6.02	0.02
Weld pad	balance	–	0.1	0.6	0.8	2.8	0.2	4.1	0.1

Table 2  
Production modes of the alloy under study

No. of sample (mode)	Ar flow rate, l/min	Amperage, A	Voltage, V	Wire feed speed, m/min	Surface cladding speed, mm/min
1	10	90–100	16.8	5.2	100
2		70–80	16.8	4.5	
3		50–60	16.8	4.0	
4		50–60	20	4.0	
5		70–80	15.8	4.5	
6		80–90	15.8	5.0	
7		70–80	14.8	4.5	
8		80–90	14.8	5.0	
9		70–80	13.8	4.5	
10		80–90	13.8	5.0	

Center using Anycubic Chiron 3D printer working on the technology of fuse deposition modeling (FDM). A Svarog MIG TECH 250 welding machine was used as a power source for surface cladding. **Table 1** shows the chemical composition of the surface cladding aluminum wire obtained from AA7075 alloy.

The surface cladding process was performed in 10 modes with a common parameter of argon flow rate  $\approx 10$  l/min and a surfacing rate of 100 mm/min (**Table 2**).

The ingot obtained according to mode 5 was cut on an DK7732 M11 jet-type electric discharge machine for further studies of phase, elemental composition and mechanical tests.

The identification of phases of the alloy was studied using X-ray phase analysis (XRD). X-ray phase analysis was carried out using X-ray diffractometer Shimadzu XRD-6000 on Cu – K $\alpha$  radiation. The lattice period was calculated from 4 peaks of the diffractogram using the equation:

$$\alpha = d_{hkl} \sqrt{h^2 + k^2 + l^2},$$

*H, K, L* – diffraction indices associated with crystallographic relations:  $H = n \cdot h, K = n \cdot k, L = n \cdot l, n$  – an integer called the reflection order.

The structure and elemental composition of the samples were studied by scanning electron microscopy (KYKY EM-6900 instrument equipped with Oxford Xplore energy dispersive analyzer). Energy dispersive X-ray spectroscopy was carried out on characteristic parts of the sample profile.

Metallographic analysis of structure changes was performed using an Olympus GX-51 optical microscope. To create optical contrast, the samples were chemically etched with the reagents: 1.5 ml of HF and 3.5 ml of distilled water.

### Results and Discussion

The initial modes for the study were the previously used surface cladding modes (mode 1–3). The use of these modes is accompanied by a fairly large splashing of metal, abundant gas emission. At the same time it should be noted that at visual measuring control a small porosity of metal is observed (pores less than 1 mm).

When the voltage is increased to 20 V (mode 4), the surface cladding process is carried out with a large amount of smoke. At the same time, aluminum burnout occurs. The cladding process is not stable and therefore not recommended for the final part production.

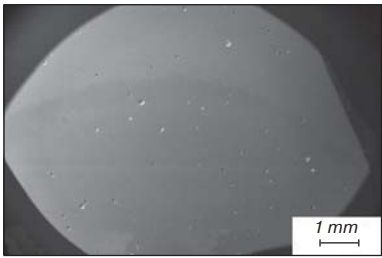
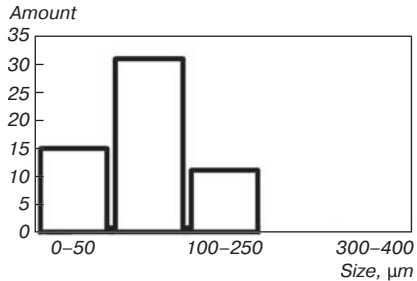
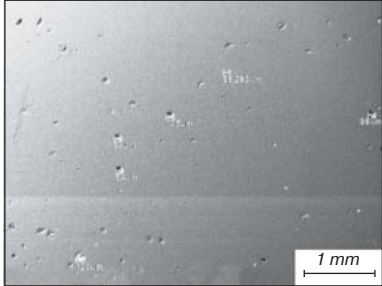
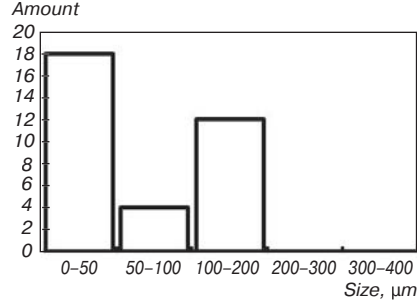
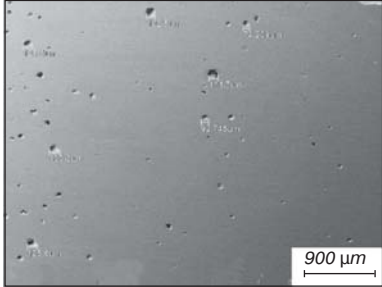
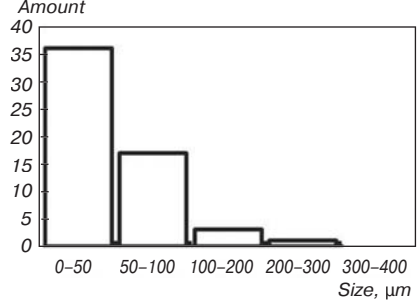
During the study of various cladding modes, the modes providing low splashing of filler material, low gas emission, as well as having good stability of the cladding process (modes 5–9) were identified. The macro-analysis of porosity of the obtained samples showed that the smallest number of large pores is observed in the

cladding materials obtained by mode No. 5 (Table 3). Therefore, the sample obtained by mode 5 was selected for the research. Fig. 1 shows the appearance of the clad layer AA7075 and characteristic zones of the study.

To study the microstructure of the fabricated workpiece, optical and electron microscopic images of the etched samples were taken and the morphology of the upper, middle and lower regions was analyzed (Figs. 2–4). Fig. 2 shows the optical and SEM images of the structure of the upper region of the clad work piece. The part has a dense and homogeneous structure with no visible cracks. The dimensional characteristics of the molding including width, height and size of the cladding were measured using a caliper. The height and width of the clad part are 50 mm and 150 mm, respectively. No traces of solidification cracks were observed and the average porosity percentage was less than 5%. Since the upper region has a higher temperature gradient due to interlayer cooling, larger and more equiaxed structures are formed (Fig. 2) with an average size of  $\approx 38.9 \mu\text{m}$ .

Fig. 3 shows the middle region. Due to the smaller temperature gradient, a mixture of columnar and dendritic equiaxed structures was formed, with an average size of  $\approx 15.5 \mu\text{m}$ . Due to the effect of heat accumulation, the dissipation becomes smaller with increasing height of the part, which leads to a decrease in the temperature gradient. Pure equiaxed grains were formed with a size of  $80 \mu\text{m}$  near the upper region of the solidified layer. A columnar grain structure was obtained near the intermediate region, which can be explained by lower heat generation. In layer-by-layer fabrication, columnar and equiaxed crystals are alternately formed near the interlayer boundary. The grain morphology was good, with an insignificant percentage of porosity. The grains formed in the clad layer have well-defined boundaries, indicating the separation of a secondary phase in the alloy, the composition of which is given in Table 4. Above the middle region, due to a smaller temperature gradient, a mixture of columnar and dendritic equiaxed structures was formed (Fig. 4). The heterogeneous secondary phase was formed around the grain boundaries and may dissolve during the fabrication process if heated repeatedly. A lower percentage of undissolved secondary phase was found near the upper and middle region to a greater extent than in the lower region.

Table 3  
Production modes of the alloy under study

Macrostructure of the faced sample	Pore distribution
<p>Mode No. 4</p> 	
<p>Mode No. 5</p> 	
<p>Mode No. 9</p> 	

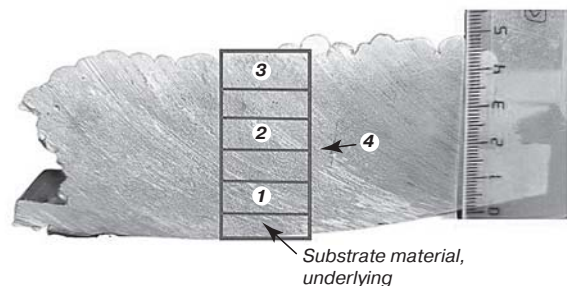


Fig. 1. Appearance of specimen No. 5 and the study area: 1 – lower area; 2 – middle area 3 – upper area; 4 – fusion zone

This indicates less thermal effects, since the secondary phases are poorly dissolved in the metal matrix. The average composition of the large number of secondary phases at the grain boundary in the studied sample is given in Table 4 and consists mainly of magnesium and zinc, precipitating in the sediment. These precipitates further hindered grain boundary movement and dissolved



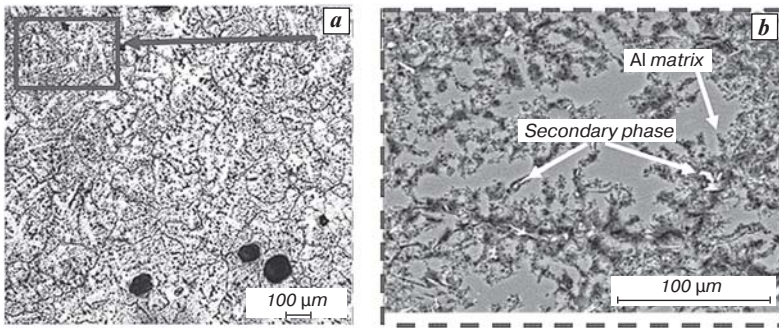


Fig. 2. Image of the upper region of AA7075: *a* – optical image; *b* – electron microscopic image

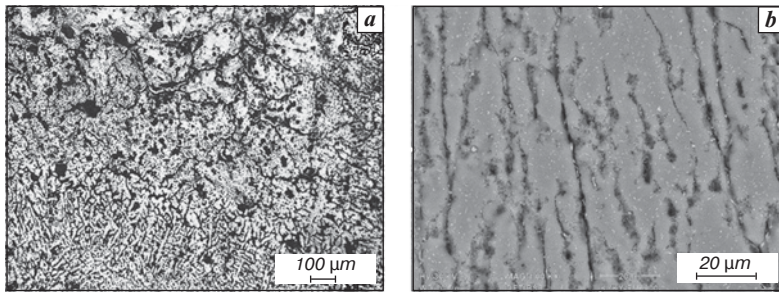


Fig. 3. Optical and electron-microscopic images of the middle region of AA7075: *a* – optical image, *b* – electron-microscopic image

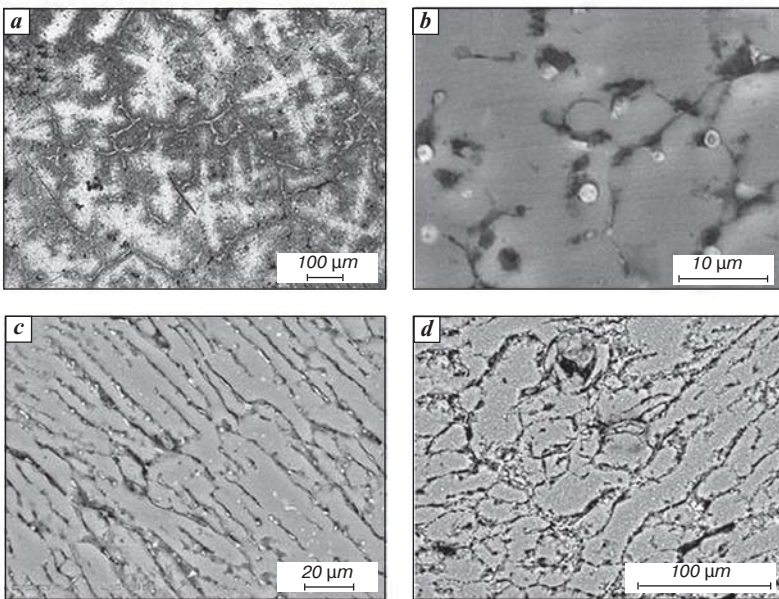


Fig. 4. Optical and electron microscopic images of AA7075: *a, b* – lower region (near the substrate); *c, d* – fusion zone

Table 4  
Result of energy dispersive analysis of investigated regions of AA7075 alloy

Elemental composition of the area	Al	Si	Fe	Mn	Cu	Mg	Cr	Zn	Ti
Matrix	balance	–	0.2	0.6	0.80	3.10	0.2	3.3	0.1
Secondary phase	balance	–	–	0.6	4.3	3.9	–	3.7	–

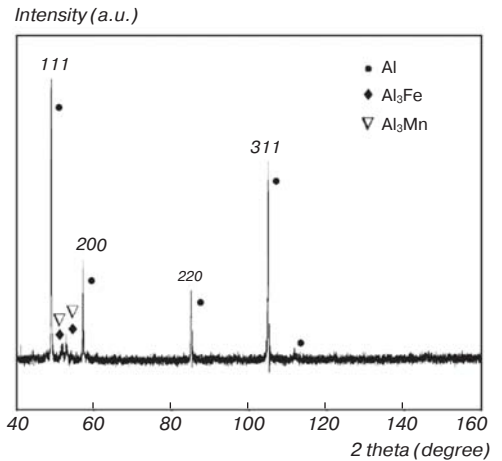


Fig. 5. X-ray diffraction of alloy AA7075

Table 5  
Lattice parameters at different values of the crystallographic plane

Crystallographic planes	Parameter <i>a</i> of the lattice, Å	Approximation error, Å
111	4.04737	0.00050
200	4.0488	0.00101
220	4.0495	0.00163
311	4.04973	0.00186
Average value	4.04787	0.00100

in the middle and lower regions due to the smaller temperature gradient (Figure 4). The secondary phase particles dissolved slowly and mixed well with Al matrix. Regarding the grain size, larger equiaxed grains were formed in the lower part than in the upper and middle regions due to repeated heat exposure. These microstructural transformations during deposition can affect the mechanical properties. Grain morphology changes with layer thickness and columnar grains predominate (Fig. 4). Equiaxed grains of  $\approx 80 \mu\text{m}$  in size are found at the layer boundaries. Although there is no noticeable change in grain size, the microstructure near the surface still has some degree of equiaxed crystalline shape.

The formation of different phases in AA7075 samples was analyzed by X-ray diffraction (Fig. 5). It was found that the main phases were Al and  $\text{Al}_3\text{Fe}$ ,  $\text{Al}_2\text{Mn}$ . The average value of the lattice parameter was  $4.048 \pm 0.001 \text{ \AA}$  (Table 5).

### Conclusion

In the present study, additively fabricated AA7075 aluminum alloy was produced using MIG welding process using constant optimum process parameters. Macroanalysis of

the selected surface cladding mode showed the lowest number of defects compared to the other modes. The microstructural properties of the obtained product were investigated layer by layer and the presence of hardening phases consisting mainly of magnesium and zinc ( $\text{MgZn}_2$ ) was established, precipitating in all areas of the studied alloy, which will prevent the growth of cracks during mechanical tensile and fatigue tests. The presence of these phases may be due to the smaller distance between primary dendrites in the aluminum matrix. The presence of columnar and dendritic equiaxed structures, the average size of which amounted to  $\sim 15.5 \mu\text{m}$ , as well as the uniform distribution of the morphology of equiaxed grains with the size of  $\sim 80 \mu\text{m}$  along the boundaries of layers of the upper and lower region of the studied alloy AA7075 were noted.

**The study was funded by the Russian Science Foundation grant No. 22-79-10245, <https://rscf.ru/project/22-79-10245/>.**

### References

- Jha A. K., Sreekumar K. Metallurgical Studies on Cracked Al – 5.5 Zn – 2.5 Mg – 1.5 Cu Aluminum Alloy Injector Disc of Turbine Rotor. *Journal of Failure Analysis and Prevention*. 2008. Vol. 8. pp. 327–332.
- Kumar P. V., Reddy G. M., Rao K. S. Microstructure, Mechanical and Corrosion Behavior of High Strength AA7075 Aluminium Alloy Friction Stir Welds – Effect of Post Weld Heat Treatment. *Defence Technology*. 2015. Vol. 11, Iss. 4. pp. 362–369.
- Isadare A. D., Aremo B., Adeoye M. O., Olawale O. J., Shittu M. D. Effect of Heat Treatment on Some Mechanical Properties of 7075 Aluminium Alloy. *Materials Research*. 2012. Vol. 16, Iss. 1. pp. 190–194.
- Mahan H. M., Konovalov S. V., Panchenko I., Al-Obaidi M. A. The Effects of Titanium Dioxide ( $\text{TiO}_2$ ) Content on the Dry Sliding Behaviour of AA2024 Aluminium Composite. *Journal of Mechanical Engineering*. 2023. Vol. 20, Iss. 3. pp. 239–261.
- Mahan H. M., Konovalov S. V., Panchenko I. Effect of Heat Treatment on the Mechanical Properties of the Aluminium Alloys Aa2024 with Nanoparticles. *International Journal of Applied Science and Engineering*. 2023. Vol. 20, Iss. 2. 2022324.
- Perry M. E. J., Rauch H. A., Griffiths R. J., Garcia D., Sietins J. M., Zhu Yunhui, Zhu Yuntian, Hang Z. Yu. Tracing Plastic Deformation Path and Concurrent Grain Refinement during Additive Friction Stir Deposition. *Materialia*. 2021. Vol. 18. 101159.
- Phillips B. J., Avery D. Z., Liu T., Rodriguez O. L., Mason C. J. T., Jordon J. B., Brewer L. N., Allison P. G. Microstructure-Deformation Relationship of Additive Friction Stir Deposition Al – Mg – Si. *Materialia*. 2019. Vol. 7. 100387.
- Pandey A. K., Chatterjee S., Siba S. Analysis and Characterisation of Weld Quality During Butt Welding Through Friction Stir Welding. *Indian Journal of Engineering & Materials Sciences*. 2019. Vol. 26, Iss. 5-6. pp. 298–310.
- Khomutov M. G., Pozdniakov A. V., Churyumov A. Yu., Barkov R. Yu., Solonin A. N., Glavatskikh M. V. Flow Stress Modelling and 3D Processing Maps of Al4.5Zn4.5Mg1Cu0.12Zr Alloy with Different Scandium Contents. *Applied Sciences*. 2021. Vol. 11, Iss. 10. 4587.
- Kermanidis A. T. Aircraft Aluminum Alloys: Applications and Future Trends. In: *Revolutionizing Aircraft Materials and Processes*. Springer International Publishing, 2020. pp. 21–55.
- Bodukuri A. K., Eswaraiah K., Rajendar K., Sampath V. Fabrication of Al – SiC –  $\text{B}_4\text{C}$  Metal Matrix Composite by Powder Metallurgy Technique and Evaluating Mechanical Properties. *Perspectives in Science*. 2016. Vol. 8. pp. 428–431.
- Pradhan S., Ghosh S., Barman T. K., Sahoo P. Tribological Behavior of Al – SiC Metal Matrix Composite Under Dry, Aqueous and Alkaline Medium. *Silicon*. 2017. Vol. 9. pp. 923–931.
- Jain P. K., Baredar P., Soni S. C. Development of Silicon Carbide Particle Reinforced Aluminium 6101 Metal Matrix Composite Using Two-Step Stir Casting. *Materials Today: Proceedings*. 2019. Vol. 18. pp. 3521–3525.
- Shalaby E. A. M., Churyumov A. Yu., Besisa D. H. A., Daoud A., Abou El-khair M. T. A Comparative Study of Thermal Conductivity and Tribological Behavior of Squeeze Cast A359/AlN and A359/SiC Composites. *Journal of Materials Engineering and Performance*. 2017. Vol. 26. pp. 3079–3089.
- Mohamed E. A., Churyumov A. Yu. Investigation of the Microstructure and Properties of Al – Si – Mg/SiC Composite Materials Produced by Solidification Under Pressure. *Physics of Metals and Metallography*. 2016. Vol. 117. pp. 1054–1060.
- Zulfia A., Raga K., Narottama W., Yunus S. Al6061 Reinforced  $\text{Al}_2\text{O}_3$  Metal Matrix Composite Produced by Double Blade Stir Casting. *International Journal on Advanced Science, Engineering and Information Technology*. 2019. Vol. 9, Iss. 5. pp. 1544–1549.
- Behera B., Dalai R., Mishra D. K., Badjena S. K. Development and Characterisation of  $\text{Al}_2\text{O}_3$  and SiC Reinforced Al – Cu Metal Matrix Hybrid Composites. *Materials Science Forum*. 2020. pp. 202–208.
- Pozdniakov A. V., Lotfy A., Qadir A., Zolotarevskiy V. S. Effect of the  $\text{B}_4\text{C}$  Content on the Structure and Thermal Expansion Coefficient of the Al – 5% Cu Alloy-Based Metal-Matrix Composite Material. *The Physics of Metals and Metallography*. 2016. Vol. 117. pp. 783–788.
- Pozdniakov A. V., Lotfy A., Qadir A., Shalaby E., Khomutov M. G., Churyumov A. Yu., Zolotarevskiy V. S. Development of Al5Cu/ $\text{B}_4\text{C}$  Composites with Low Coefficient of Thermal Expansion for Automotive Application. *Materials Science and Engineering: A*. 2017. Vol. 688. pp. 1–8.
- Pozdniakov A. V., Zolotarevskiy V. S., Barkov R. Y., Lotfy A., Bazlov A. I. Microstructure and Material Characterisation of 6063/ $\text{B}_4\text{C}$  and 1545K/ $\text{B}_4\text{C}$  Composites Produced by Two Stir Casting Techniques for Nuclear Applications. *Journal of Alloys and Compounds*. 2016. Vol. 664. pp. 317–320.
- Lotfy A., Pozdniakov A. V., Zolotarevskiy V. S., Abouel-khair M. T., Daoud A., Mochugovskiy A. G. Novel Preparation of Al5%Cu / BN and Si3N4 Composites with Analysing

Microstructure, Thermal and Mechanical Properties. *Materials Characterization*. 2018. Vol. 136. P. 144–151.

22. Shalaby E. A. M., Churyumov A. Yu., Solonin A. N., Lotfy A. Preparation and Characterisation of Hybrid A359/(SiC + Si<sub>3</sub>N<sub>4</sub>) Composites Synthesised by Stir/Squeeze Casting Techniques. *Materials Science and Engineering: A*. 2016. Vol. 116. pp. 847–861.

23. Alekseev A. V., Yesikov M. A., Strekalov V. V., Mali V. I., Khasin A. A., Predtechensky M. R. Effect of Single Wall Carbon Nanotubes on Strength Properties of Aluminum Composite Produced by Spark Plasma Sintering and Extrusion. *Materials Science and Engineering: A*. 2020. Vol. 793. 139746.

24. Zhang X., Li S., Pan B., Pan D., Liu L., Hou X., Chu M., Kondoh K., Zhao M. Regulation of Interface Between Carbon Nanotubes/aluminum and Its Strengthening Effect in CNTs Reinforced Aluminum Matrix Nanocomposites. *Carbon*. 2019. Vol. 155. pp. 686–696.

25. Lotfy A., Pozdniakov A. V., Zolotarevskiy V. S., Mohamed E., el-Khair M. T. A., Daoud A., Fairouz F. Microstructure, Compression and Creep Properties of Al – 5% Cu –

0.8 Mn/5% B<sub>4</sub>C Composites. *Materials Research Express*. 2019. Vol. 6, Iss. 9. 095530.

26. Chawla N., Chawla K. K. *Metal Matrix Composites*. 2<sup>ed</sup>. Springer: New York, 2022. XVI+370 p.

27. Ding W., Cheng Y., Chen T., Zhao X., Liu X. Research Status and Application Prospect of Aluminum Matrix Composites. *Research and Application of Materials Science*. Vol. 2, Iss. 1. pp. 23–33.

28. Muthukrishnan N., Davim J. P. Optimisation of Machining Parameters of Al/SiC-MMC with ANOVA and ANN Analysis. *Journal of Materials Processing Technology*. 2009. Vol. 209, Iss. 1. pp. 225–232.

29. Taştan M., Gökozan H., Çavdar P. S., Soy G., Çavdar U. Analysis of Artificial Aging with Induction and Energy Costs of 6082 Al and 7075 Al Materials. *Revista de Metalurgia*. 2009. Vol. 55, Iss. 1. 137.

30. Xia H., Zhang L., Zhu Y., Li N., Sun Y., Zhang J., Ma H. Mechanical Properties of Graphene Nanoplatelets Reinforced 7075 Aluminum Alloy Composite Fabricated by Spark Plasma Sintering. *International Journal of Minerals, Metallurgy and Materials*. 2020. Vol. 27, Iss. 9. pp. 1295–1300. 